Electrowetting Phenomenon on Nanostructured Surfaces Studied by Using Atomic Force Microscopy

ARTICLE *in* THE JOURNAL OF PHYSICAL CHEMISTRY C · JUNE 2012

Impact Factor: 4.77 · DOI: 10.1021/jp301549p

THE JOURNAL OF PHYSICAL CHEMISTRY C

Article

pubs.acs.org/JPCC

Electrowetting Phenomenon on Nanostructured Surfaces Studied by Using Atomic Force Microscopy

Reynier I. Revilla,[†,§] Li Guan,[†,‡] Xiao-Yang Zhu,[†] Bao-Gang Quan,[†] Yan-Lian Yang,*[,†] and Chen Wang*[,†]

[†]Key Laboratory of Standardization and Measurement for Nanotechnology (Chinese Academy of Sciences), National Center for Nanoscience and Technology, Beijing 100190, P. R. China

[‡]Department of Chemistry, Renmin University of China, Beijing 100872, P. R. China

[§]Centro de Estudios Avanzados de Cuba, La Habana 19370, Cuba

Supporting Information

ABSTRACT: An electrowetting (EW) phenomenon was studied using atomic force microscopy (AFM) on poly(methyl methacrylate) (PMMA) surfaces with nanostructures formed by lithography treatment or covered with a thin layer of titanium dioxide (TiO_2) nanoparticles. By measuring the adhesion force, as well as its magnitude of fluctuations, between the conductive AFM tip and the dielectric surface at different electric fields, the characteristic EW features could be identified. By comparison of the EW characteristics on smooth PMMA surface with that on a lithographically patterned or TiO_2-nanoparticle covered PMMA surface, the impact of the three-phase contact line and dielectric properties on the EW phenomena could be demonstrated. It reveals that the transition from ideal EW to EW saturation is associated with intrinsic dielectric properties rather than with the solid−liquid interface characteristics. The second transition from EW saturation to EW breakdown could be attributed to changes in the three-phase contact line.

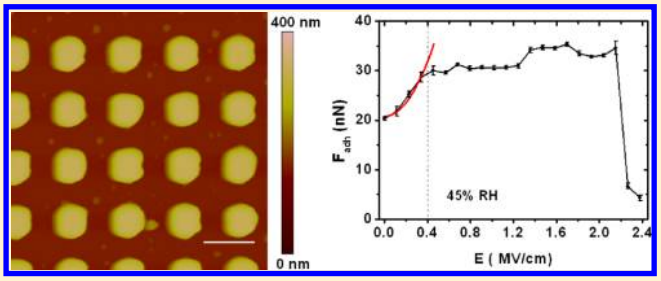

1. INTRODUCTION

Wetting properties of a given system can be tuned by surface modification or chemical doping. Electrowetting (EW) has long been known to affect the contact angle without changing the chemical composition of the contacting phases. EW is the phenomenon of contact angle decrease under the influence of an external voltage applied across the solid/liquid interface, or the use of electric fields to improve the wetting of a dielectric surface. EW has several practical applications such as adjustable lens[1−3] for miniature systems, controlled liquid transportation in microchannels,[4−7] and micro-total-analysis system for clinical diagnostics.[8] EW can also be used to deliver and mix microliter or nanoliter volumes of liquid droplets with relatively low electrical potential.[9,10] Currently, the research interest in EW is also increasing for understanding the effect of electric field on interfacial properties of water, since comparatively high electric fields may exist in and influence transport through ion channels of cell membranes. The EW phenomenon is also crucial for the electric power transmission lines to induce potential flashover, which is one of the main reasons for power failure disasters.

The fundamental understanding of EW phenomenon has been extensively pursued especially at the length scale of micro- and nanometers with the motivation from various applications in nanosensors, microfluidic devices, etc. The dynamics of the three-phase contact line for characterization of the wetting process has been a subject of many recent studies.[4−7,11−16] The common experimental configuration in the electrowetting study consists of a drop of electrolyte solution resting on top of an electrode insulated with a thin polymer layer. The equilibrium contact angle, θ, at the three-phase contact line is given by the well-known Young−Lippmann equation

$$\cos\theta = \cos\theta_0 + \frac{1}{2}\frac{C}{\gamma}V^2 \quad (1)$$

where V is the applied voltage, C is the capacitance per unit area of the insulating layer, θ_0 is the contact angle at zero external voltage, and γ is the liquid interfacial tension. It is largely accepted that eq 1 provides a good description of the electrowetting phenomenon[4,5,17,18] as long as the voltage does not exceed a certain threshold. Beyond this threshold, the contact angle remains constant (unaffected by the increasing voltage), for which different explanations have been proposed such as dielectric breakdown, charge trapping,[19,20] droplet resistance,[21] zero interfacial tension criterion,[22] and gas ionization in the vicinity of the contact line, while rigorous agreement among these mechanisms has yet to be reached.

Wetting phenomena, in general, have been shown to be affected by the drop size as well as the feature size at the liquid/solid interface. Some theoretical studies have shown a high dependence of the contact angle on the drop size at nanometer scale,[23] and the polarity and direction of the electric field.[24−27]

Received: February 16, 2012
Revised: June 12, 2012
Published: June 18, 2012

dx.doi.org/10.1021/jp301549p | J. Phys. Chem. C 2012, 116, 14311−14317

The wetting and electrowetting properties can be altered by constructing nanostructured surfaces, which have been mainly studied by monitoring the apparent contact angle.[11,18,28−31]

Atomic force microscopy (AFM) is a powerful tool for providing high-resolution topographic information and detecting sensitive interaction forces at nanoscale. AFM is also a very important tool for investigating thin liquid films[32] and confined liquids with the ability of tracing force in gaseous or liquid environment.[32−34] Force spectroscopy and friction force microscopy have been utilized to provide complementary information about the EW effect.[35,36] Although a biased tip could pull the sample surface when this is retracted from it (see Figure S1 of the Supporting Information),[37] we believe that the influence from the pattern formation in our measurements could be neglected because of the following reasons. The lateral dimensions of the pattern (from 380 to 420 nm) induced in the sample surface by the biased tip are much larger than the tip radius (∼10 nm) in our case (see Figure S1 of the Supporting Information) and the tip contact at the surface around the middle of the pattern. These patterns have an apparent height ranging from 35 to 45 nm which could also be contributed from the electrostatic force associated with the charge injection. In addition, the adhesion force arises from the breaking of the water meniscus which is far above the top of the pattern; thus, the contribution of the pulling force of the tip from the surface could be neglected. From the above discussion, we believe that the influence from the pattern formation in our measurements should not be substantial. By measuring the local adhesion force between AFM tip and the surface,[35] the EW phenomenon is observed to be closely related to the contact angle under medium electric field. In the ideal EW region (lower electric field), the total adhesion can be expressed as a function of the applied voltage similar to Young−Lippmann equation[35]

$$F_{adh} = c_1 + c_2 V^2 \quad (2)$$

where c_1 and c_2 are constants that depend on the dielectric layer, the liquid layer, and the tip characteristics.

The nanometer scale distance between tip and sample gives rise to a very high electric field, which permits the investigation of EW phenomenon at extremely high electric fields. In contrast, it is difficult to obtain such high electric fields in measuring the macroscopic contact angle. In our previous reports,[35,36] a dramatic decrease in adhesion force and abrupt increase of the error in friction force measurements were identified under high electric field, which may be associated with the breakdown of the capacitive layer formed by the water film and dielectric layer or polarization of water molecules at the interface. The nearly flat dielectric film surface in the previous report[35] only allowed us to focus on the impact of the electric field on the EW mechanism. Considering the significance of the three-phase contact line, we focus here on the EW phenomenon at liquid−dielectric interface with nanostructures by using AFM technique, which could give hints to nanoscale EW behavior. Nanostructured surfaces for changes in the liquid−dielectric interface can result in different electric field orientations at the three-phase contact line and also the interfacial polarization, which in turn can affect the EW at the interface. The present work is an extension of our previous study[35] in which the force spectroscopy method is also applied to study the EW effects at nanometer scale.

In the present study, the EW phenomena were observed by measuring the local adhesion force between the AFM tip and the PMMA surfaces with different structures. The lithographically patterned PMMA surface and the flat PMMA surface covered with a thin layer of titanium dioxide (TiO_2) nanoparticles were considered for studying changes in the three-phase contact line with submicrometer and nanometer sized surface structures. The influences of the modified PMMA surfaces on EW phenomena were studied from the viewpoint of three-phase contact line and the tip−sample capacitance. The transition from ideal EW to EW saturation seems to be related to the intrinsic dielectric properties of the dielectric film. Differences in the transition that lead to the drastic decrease in the adhesion force compared with the previously reported results[35,36] could be associated with the changes in the three-phase contact line.

2. EXPERIMENTAL DETAILS

2.1. Patterned PMMA Sample. The patterned PMMA sample used in the experiment was fabricated by using electron beam lithography (EBL) technique. A bilayer of PMMA (Alfa Aesar)/PMMA 950k (Allresist AR-P 679.04) resist, with the PMMA being insensitive to electrons and PMMA 950k generally used as an electron resist, was spin-coated onto a silicon wafer for pattern formation. First, a 140 nm PMMA film was spin-coated on Si (100) substrate (from Silicon Quest International) doped with phosphorus (2−4 Ω cm) and followed by soft-bake at 180 °C for 1 min. Then, 180 nm PMMA 950k film was spin-coated on the PMMA layer and soft-baked at 180 °C for 1 min. EBL was carried out using an SEM (JEOL 5900) converted to EBL system under 30 kV acceleration voltage, with a working distance of 5 mm. PMMA island array with approximately 500 nm in diameter and 1 μm in periodicity was fabricated.

2.2. PMMA Film Covered with a Thin Layer of TiO_2 Nanoparticles. In order to prepare the PMMA film covered with a thin layer of TiO_2 nanoparticles, a thin film of PMMA (650 nm thick) was first prepared by spin-casting PMMA (Alfa Aesar) solution in chlorobenzene on Si(100) substrate followed by solvent evaporation at 90 °C for 5 h. TiO_2 nanoparticles (Aeroxide T805) with diameter of approximately 21 nm were purchased from Degussa, which were fumed titanium dioxide treated with octylsilane to achieve a hydrophobic surface. The TiO_2 nanoparticles were dispersed in ethanol and drop-cast on top of the PMMA film.

2.3. AFM Characterization. The local adhesion behavior was studied using the force spectroscopy method of AFM conducted with a commercial AFM (Dimension 3100, Nanoman II, Bruker). V-shaped cantilever coated with thin layers of Cr and Au, with a nominal spring constant of 3 N/m and a nominal radius of 50 nm (MikroMasch), was used as the top electrode and used to measure the local adhesion force between the tip and the sample surface. The adhesion forces at different applied voltages were measured on the same sample location using the same tip in order to avoid variations related to different tip geometries. There were 1000 force−distance curves obtained at each applied voltage for determination of the average adhesion force and the standard deviation by Gaussian fitting of the histograms of the adhesion forces. Measurements were conducted within 8 min in order to be consistent during the application of different values of the applied voltage. In all the cases the substrate was grounded while the voltage was applied to the tip. During the measurements the magnitude of the adhesion force and its behavior for different values of the applied voltage were not influenced by the tip velocity within the range from 4 to 8 μm/s. Measurements were carried out

with a tip velocity of 7.75 μm/s. The maximum cantilever deflection was kept relatively small during measurement, typically about 200 nm, in order to avoid damage in the sample surface as is shown in Figure S2 of the Supporting Information.

The behavior of the adhesion force for different values of the applied voltage was found to be approximately the same when the relative humidity ranged from 40% to 65%. Thus, experiments were always conducted within that RH range.

In order to obtain the topography of the sample and measure the surface roughness, experiments were performed in tapping mode using a square pyramidal silicon tip with a nominal radius of 10 nm on a rectangular Si(100) cantilever at a resonance frequency of 255 kHz (RTESP, Veeco Instruments).

2.4. Contact Angle Measurement. The macroscopic contact angles of water on PMMA surface and TiO_2 nanoparticles covered PMMA surface were measured using a contact angle measurement instrument (DSA100, Krüss). For each value 20 drops were analyzed with a volume of approximately 3 μL.

2.5. Resistance Measurement. The electrical resistance of PMMA was measured using a Milli-Q water droplet resting on top of a smooth PMMA surface with a subfemtoamp remote source meter (Keithley 6430).

3. RESULTS AND DISCUSSION

3.1. Electrowetting on Patterned PMMA Surface. PMMA is a dielectric polymer widely used in MEMS/NEMS devices; thus, it is very important to study the EW phenomenon on this surface. By fabricating a patterned PMMA surface, the influence of the three-phase contact line on the EW behavior can be studied. This might be especially important when micro- and nanodevice applications are involved. The topographic image of the patterned PMMA surface is shown in Figure 1a with periodicity of 1 μm, pitch width of 580 nm, and height of 160 nm on PMMA/PMMA 950k bilayers. The sidewalls of the patterns are not steep, perhaps due to the dispersion of the etching process and the AFM tip convolution effect.

Patterned PMMA surfaces are expected to exhibit a reduced macroscopic contact angle compared with the smooth surface.[38] The contact angles of the rough surface and the smooth surface of the same material are related through the Wenzel[39] or Cassie[40,41] equation depending on the relative dimensions of the roughness. Both equations show a linear dependence between the cosines of the angles. In the case of the patterned PMMA surface, roughness dimensions are larger than the dimensions of the tip; hence, Wenzel and Cassie effects were not taken into account. It should be noted that the roughness dimensions are not large enough to completely ignore their influence on the meniscus geometry or on the surface electric field distribution.

From the tapping mode AFM image (Figure 1a), the average thickness of the patterned PMMA film can be estimated to be about 260 nm. The average electric field strength E can be obtained as $\langle E\rangle = V/\langle d\rangle$, as a very rough estimation, where V is the applied voltage and d the average dielectric thickness. In any case, $\langle E\rangle$ is proportional to the applied voltage. The rigorous determination of the magnitude of the electric field in the patterned PMMA film should require quantitative details of geometry of the tip and surface features, dielectric distributions, etc., and is a nontrivial task.

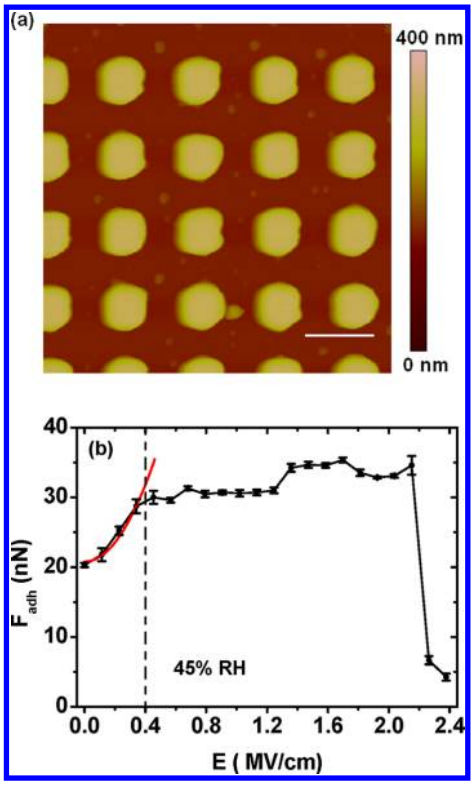

Figure 1. (a) Tapping mode AFM image of patterned PMMA surface. The scan size is 5 μm × 5 μm (scale bar = 1 μm). (b) Total adhesion force between the AFM conductive tip and the patterned PMMA surface versus the external applied electric field, under 45% environmental relative humidity (RH). The red line is the parabolic fit to the data.

The adhesion force between the AFM tip and the patterned PMMA surface as a function of the applied electric field is plotted in Figure 1b. It can be observed that the total adhesion force follows approximately a quadratic behavior when the electric field is lower than 0.35 MV/cm, which can be called the ideal EW region in accordance with the Young−Lipmann equation.[35] With the increase of the applied external voltage, a notable deviation in the adhesion force from the quadratic behavior can be observed above 0.35 MV/cm. The total pull-off force still increases slightly with the external voltage but is considerably lower than that predicted by the quadratic behavior, which may be due to the EW saturation.[35] A sharp decrease of the adhesion force can be found when the electric field is above 2.2 MV/cm, which we referred to as the EW breakdown effect.[35]

According to previous reports,[42,43] the total capillary force between two solid surfaces follows the equation

$$F_{cap} = \gamma \cdot l - \Delta P \cdot S \tag{3}$$

where l and S are the perimeter of the cross-sectional surface and the cross-sectional area of the meniscus, respectively, γ is the surface tension of the liquid−gas interface, and ΔP is the pressure difference due to the curved surface of the liquid condensed between the two solid surfaces. ΔP depends on the exact geometry of the liquid meniscus. Since it is impossible to know the exact shape of the meniscus, the equation to describe the capillary force can only be obtained for few and very specific surface geometries, considering some approximations. Capillary force equations obtained for different radial symmetric

dx.doi.org/10.1021/jp301549p | J. Phys. Chem. C 2012, 116, 14311−14317

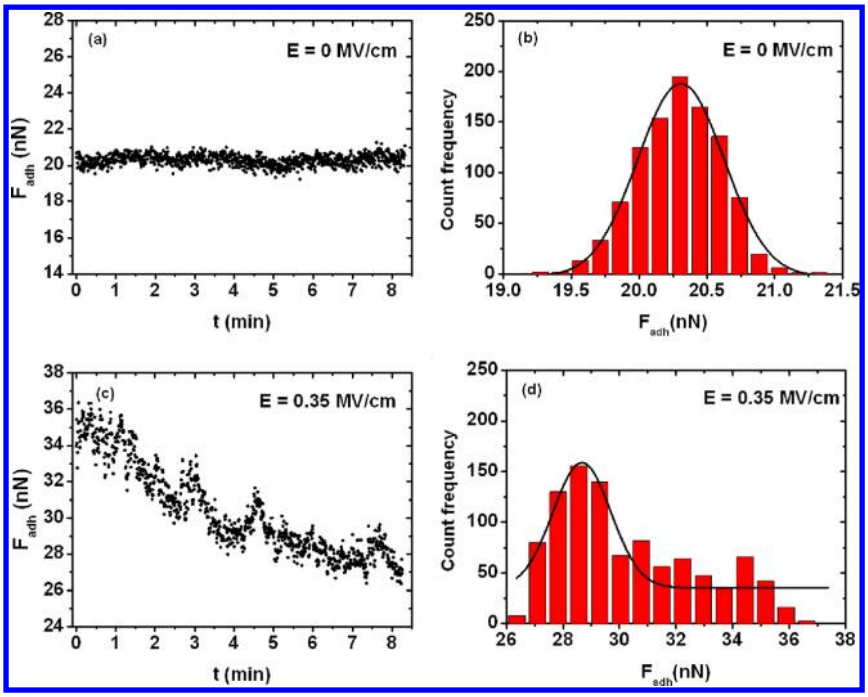

Figure 2. Time dependence of the total adhesion force between the conductive AFM tip and the patterned PMMA surface during measurement (a and c) together with the Gaussian fitting to the histogram of 1000 adhesion force values (b and d). The external applied electric field values are 0 MV/cm (a and b) and 0.35 MV/cm (c and d).

geometries[42] show a linear dependence with respect to the cosine of the contact angle between the liquid and the solid surface, which means a quadratic dependence on the applied voltage (eq 1). Considering AFM tips with spherical shape in the end (spherical symmetry), a quadratic dependence of the adhesion force (capillary force) on the applied voltage can be expected as a first approximation.

In the ideal EW region, a quadratic behavior can be described by fitting a parabola equation (eq 2), F_{adh}= 20.79 + 0.102 V^2 (F_{adh} given in nN and V in volts), with an R^2 of 0.967. The coefficient c_2 in eq 2 was similar to the one in the previous result (0.082),[35] on a smooth PMMA surface, which confirms the strong dependence of coefficient c_2 on the capacitance of the system, which is determined by the capacitance of the dielectric.

The electric field at the EW saturation (deviation from the quadratic behavior) point is estimated to be about 0.35 MV/cm for the patterned PMMA surface, similar to the value for smooth PMMA surface (~0.4 MV/cm),[35] which suggests that the transition from ideal EW to EW saturation is less dependent on changes in the three-phase contact line, while depending predominantly on the dielectric properties of the materials.

With the electric field ranging from 0.35 to 0.45 MV/cm, larger measurement fluctuations were clearly recognized, which are indicated as the standard deviation. As shown in Figure 1b, the value of the standard deviation is larger for those values of the adhesion force close to the regions where changes in the adhesion force are observed. Larger standard deviation, in general, suggests the idea of instability in the system, frequently related to transition processes. Therefore, transition from ideal electrowetting region (quadratic behavior) to saturation region can be identified on the basis of the abrupt change in measured signal fluctuations. The idea of instability can be confirmed in Figure 2, which reveals the time dependence of the adhesion force during measurement in approximately 8 min without (a) and with (c) application of external electric field of 0.35 MV/cm. Figure 2a shows a relatively stable adhesion force at 0 electric field, while magnified fluctuations in the adhesion force are easily identified in Figure 2c. Several experimental factors could affect the adhesion force, such as contact area between tip and sample and number of water molecules within one contact, among others. All those factors have inevitable variations from independent measurements, thus Gaussian fitting was applied to reflect the distribution and the variations. The observed larger standard deviation indicates the wide distribution of the adhesion forces including the slight drift of the adhesion force and also the variation in contact conditions. Although several peaks were observed during the adhesion force measurements at the transition points, there was no characteristic periodicity that can be identified. However, one thing that could be concluded from this is that the electrowetting saturation seems to be a time dependent phenomenon.

It can be observed that the measured pull-off force remains approximately constant when the applied electric field is within the range from 0.6 to 1.3 MV/cm (Figure 1b). Around 1.3 MV/cm the adhesion force undergoes a change to a higher value and then remains nearly constant until 2.2 MV/cm. Within the range from 0.6 to 2.2 MV/cm the standard deviations of the adhesion forces are relatively low. As the patterned surface was fabricated by spin-casting two layers of PMMA, at extremely high external electric field the system might become unstable and loosening of some of the polymer species may occur, causing variations in the measured adhesion force. This could be due to the extremely high electric field generated at this scale, which can cause electrostatic deformation, nanoexplosion (when the tip is biased, the electric field exceeds the breakdown strength of dielectrics, initiating the explosive discharge of the air/water media in the tip–substrate gap), and shock wave generation.[37] The region from

0.6 to 2.2 MV/cm is identified as the complete saturation region, which has also been observed previously.[35,36]

With further increasing the applied external electric field until it reaches a value above 2.2 MV/cm, a drastic decrease in the adhesion force can be observed (Figure 1b), which has been reported for the smooth PMMA surface in our previous work.[35] The adhesion force measured at an external electric field of 2.2 MV/cm shows a larger standard deviation value, which is also observed by friction force microscopy.[36] The estimated electric field value ($\langle E \rangle$ = 2.2 MV/cm) at the point where the transition was observed is much higher than the value reported ($\langle E \rangle$ = 1.1 MV/cm) using a smooth PMMA surface sample.[35,36] By changing the surface structure (increasing the surface roughness), an increase in the electric strength associated with the EW breakdown was detected. Because the only difference between the smooth surface and the patterned surface is the structure, this could lead to the changes in three-phase contact line at the edges of the troughs and the protrusions. Thus, the variation in this electric field threshold for EW breakdown (second transition) might be dependent on the changes in three-phase contact line. The increased EW breakdown electric field could benefit the droplet control and flow control in nanodevices and microfluidic devices by changing the surface roughness and patterning.

3.2. Electrowetting of PMMA Film Covered by Thin Layer of TiO_2 Nanoparticles. It is challenging to obtain a patterned polymer surface with tens of nanometers by lithography techniques. Herein, we prepared the nanostructures surface by covering the surface with nanoparticles. Particles of titanium dioxide with average radius of 25 nm were used to cover the surface of approximately 650 nm thick PMMA film, resulting in a surface structure with nanometer scale corrugations. The relative dielectric constant of the TiO_2 is around 85, much higher than the relative dielectric constant of the PMMA (from 2.5 to 4). Thus, the capacitance of the system composed by the PMMA and the TiO_2 film is mainly determined by the capacitance of the PMMA, as it is in the case of two capacitors in a parallel configuration (the capacitor with the lower capacitance determines the overall capacitance). Then, the impact can be discussed on the basis of the nanoscale roughness, not the capacitance change. The electric field in this case was roughly estimated considering only the thickness of the PMMA film.

The measured water contact angle on PMMA surface was 68° ± 2.1°. After depositing the TiO_2 nanoparticles the water contact angle of the new surface was 84° ± 4°. The slight increase of the contact angle may be associated with the octylsilane functionalization on the nanoparticle surface. The surface roughness may also contribute to the contact angle changes.[38−41]

The topographic image of the surface is shown in Figure 3a. By using tapping mode AFM, the root-mean-square (rms) roughness of the PMMA surface was obtained at about 0.27 nm (scan size of 2 μm × 2 μm), and after the thin layer of TiO_2 nanoparticles was deposited the rms roughness was 0.98 nm.

The dependence of adhesion force on the applied electric field on PMMA surface covered with TiO_2 nanoparticles is shown in Figure 3b. It can be noted that when the applied electric field is lower than 0.31 MV/cm, the relationship between the adhesion force and the applied voltage follows a quadratic characteristic, as is described in eq 2. In this region F_{adh} = 13.89 + 0.1009 V^2 (F_{adh} given in nN and V in volts), with an R^2 of 0.985. The value of the constant c_2 is very similar to

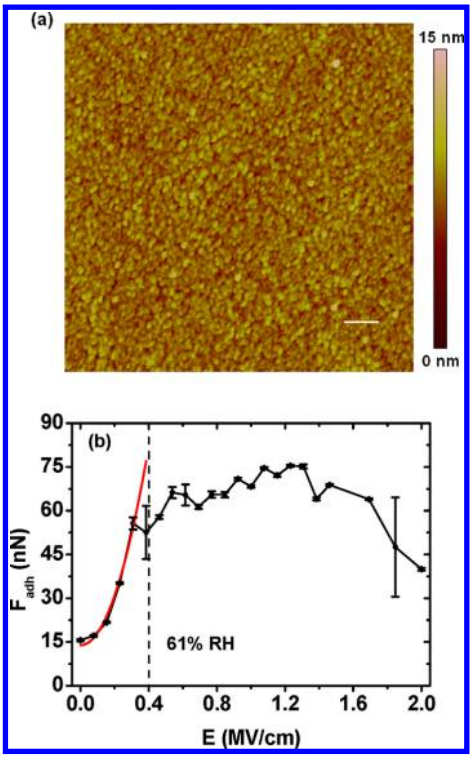

Figure 3. (a) Tapping mode AFM image of PMMA surface covered with TiO_2 nanoparticles. The scan size is 2 μm × 2 μm (scale bar = 200 nm). (b) Total adhesion force between the AFM conductive tip and the PMMA surface covered with TiO_2 nanoparticles versus the external applied electric field, under 61% environmental relative humidity (RH). The red line is the parabolic fit to the data.

those obtained with the patterned (0.102) and smooth PMMA surfaces (0.082). Even though it was a different solid−liquid interface, this further confirms the direct and strong dependence of c_2 on the dielectric capacitance and in general the transition from the ideal EW to the EW saturation.

When the applied electric field is around 0.4 MV/cm, standard deviation in the pull-off force increases compared to those values associated with lower electric field strengths. In Figure 4 the instability of the adhesion force at 0.4 MV/cm can be clearly observed. The consistency of the first EW transition point from ideal EW to EW saturation for the three surfaces confirms that changes in the three-phase contact line do not play an important role in the saturation effect. The EW saturation phenomenon seems to be associated with intrinsic dielectric properties of the dielectric layers.

The total adhesion force significantly deviates from the quadratic behavior (Figure 3b) for values of the applied electric field above 0.4 MV/cm. The saturation region can be identified by external electric field values between 0.5 and 1.7 MV/cm. The total adhesion force drastically decreases with increasing the applied electric field above 1.7 MV/cm (Figure 3b). The standard deviation in the adhesion force is relatively low in the saturation region, which confirms that there is no transition within this electric field interval (from 0.5 to 1.7 MV/cm), and hence, these points belong to the same region. Small variations in the adhesion force observed in the saturation region may be associated with changes in the surface structure, such as the migration of nanoparticles due to high electric field. The difference between 1.1, 1.7, and 2.2 MV/cm for the second

dx.doi.org/10.1021/jp301549p | J. Phys. Chem. C 2012, 116, 14311−14317

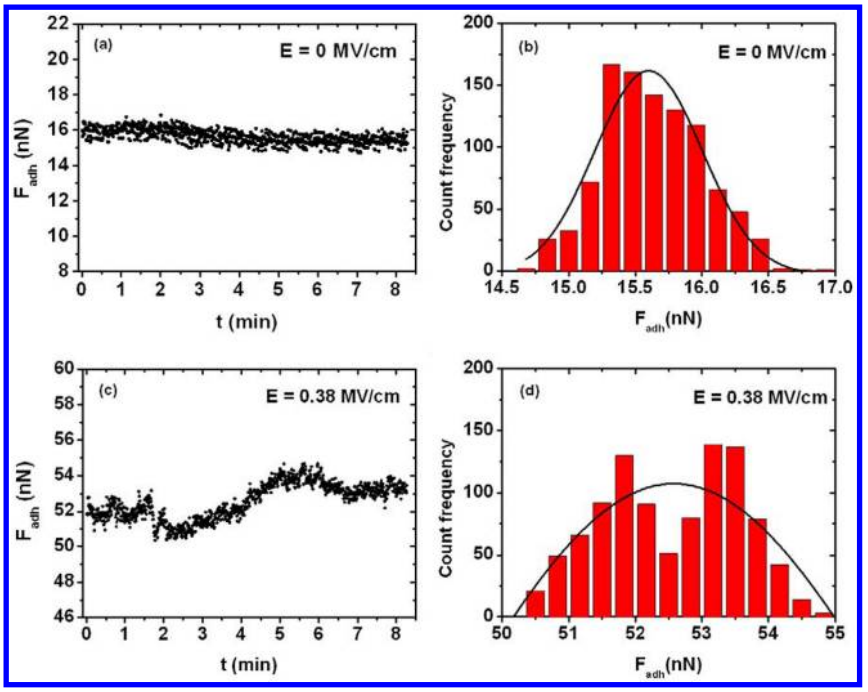

Figure 4. Time dependence of the total adhesion force between the conductive AFM tip and the PMMA surface covered with TiO_2 nanoparticles during measurement (a and c) together with the Gaussian fitting to the histogram of 1000 adhesion force values (b and d). The external applied electric field values are 0 MV/cm (a and b) and 0.38 MV/cm (c and d).

transition in EW effect could be related to the increase of the surface roughness to change the three-phase contact line.

In order to further confirm the impact of intrinsic dielectric property and the three-phase contact line on the EW, electrical resistance measurement on the PMMA film was carried out. By using a macroscopic electrowetting setup, the electrical resistance of the system was measured while an electric field was applied (Figure 5a). It can be noted in Figure 5b that at about 0.4 MV/cm the electrical resistance drastically decreases,

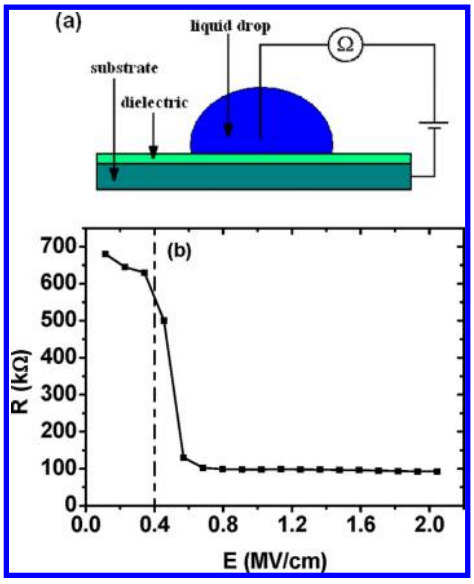

Figure 5. (a) Electrowetting setup with a Milli-Q water droplet resting on top of a smooth PMMA surface with 0.27 nm surface roughness. While an external electric field is applied, the electrical resistance of the system is measured. (b) Electrical resistance of the system under different external applied electric field values.

which confirms the dielectric breakdown[44] as the possible explanation for the saturation effect. The result further confirms that the intrinsic dielectric property is predominant at the first transition. It can also be noted that the electrical resistance of the electrowetting system remains constant above 0.7 MV/cm applied electric field, which indicates less dependence of the EW on the dielectric properties of the film at extremely high electric field. Considering the dependence of the electric field at transition points on the surface morphologies in all the three cases, the second transition may be dominated by changes at the liquid−solid interface, i.e., the three-phase contact line.

The second transition in the adhesion force is observed in Figures 1b and 3b at extremely high electric field values, even higher than the value at which water molecule polarization has been observed in previous studies.[24] Polarization of water molecules at the liquid−solid interface might depend on the specific interface geometry because the orientation and the magnitude of the electric field can be different at the sharp edges and points. The electric field variations at the second transition for surfaces with different roughness in this report might indicate association of the EW breakdown with the polarization of water molecules.

4. CONCLUSIONS

The electrowetting phenomena on patterned PMMA surfaces were studied using force spectroscopy method of AFM. The total adhesion force showed an approximately quadratic dependence on the external applied voltage for low values of the electric field ($\langle E \rangle$ < 0.4 MV/cm) for all the surfaces. The similar c_2 values in the ideal EW region and the similar transition points from ideal EW to EW saturation (~0.4 MV/cm) were observed for all the cases (smooth PMMA surface, nanoparticle covered PMMA surface, and patterned surface with submicrometer feature), which indicates this transition is dominated by the intrinsic dielectric properties. At extremely

high electric field values, we observed a drastic decrease in the adhesion force which refers to the EW breakdown. The great difference between second transition points, from EW saturation to EW breakdown, may be attributed to the changes in the three-phase contact line, which will shed light on the surface structure design for the dielectric layers in power transmission at extremely high electric fields, or for tunable lenses and micro-total-analysis systems operated at high electric fields. The two case studies could help illustrate the effects of surface structures on EW phenomenon. Systematic studies on the pattern size, feature height, pattern spacing, and various dielectric layers with different dielectric constant are highly desired in the future for better understanding of the EW mechanism at nanoscale.

■ ASSOCIATED CONTENT

Supporting Information

AFM topography images of a flat PMMA surface after obtaining 1000 force-curve with different values of the voltage applied to the tip and AFM topography images of a flat PMMA surface after obtaining 1000 force-curve with different cantilever deflection. This material is available free of charge via the Internet at http://pubs.acs.org.

■ AUTHOR INFORMATION

Corresponding Author

*Phone: 86-10-82545561. Fax: 86-10-62656765. E-mail: wangch@nanoctr.cn (C.W.), yangyl@nanoctr.cn (Y.-L.Y.).

Notes

The authors declare no competing financial interest.

■ ACKNOWLEDGMENTS

Financial support from the National Natural Science Foundation of China (Grant 20873033) and National Key Project for Basic Research (Grants 2011CB932800, 2007CB936800) is gratefully acknowledged. R.I.R. also acknowledges the financial support from the Ministry of Science and Technology of China (MOST).

■ REFERENCES

(1) Hou, L.; Smith, N. R.; Heikenfeld, J. *Appl. Phys. Lett.* **2007**, *90*, 251114−251116.
(2) Bergea, B.; Peseux, J. *Eur. Phys. J. E: Soft Matter Biol. Phys.* **2000**, *3*, 159−163.
(3) Yang, S.; Krupenkin, T. N.; Mach, P.; Chandross, A. *Adv. Mater.* **2003**, *15*, 940−943.
(4) Blake, T. D.; Clarke, A.; Stattersfield, E. H. *Langmuir* **2000**, *16*, 2928−2935.
(5) Decamps, C.; De Coninck, J. *Langmuir* **2000**, *16*, 10150−10153.
(6) Kuo, J. S.; Spicar-Mihalic, P.; Rodriguez, I.; Daniel, T. *Langmuir* **2003**, *19*, 250−255.
(7) Müller, P.; Kloss, A.; Liebetraut, P.; Mönch, W.; Zappe, H. *J. Micromech. Microeng.* **2011**, *21*, 125027−125040.
(8) Mugele, F.; Baret, J.-C. *J. Phys.: Condens. Matter* **2005**, *17*, R705−R774.
(9) Prins, M. W. J.; Welters, W. J. J.; Weekamp, J. W. *Science* **2001**, *291*, 277−280.
(10) Lee, J.; Moon, H.; Fowler, J.; Schoellhammer, T.; Kim, C.-J. *Sens. Actuators, A* **2002**, *95*, 259−268.
(11) Krupenkin, T. N.; Taylor, J. A.; Schneider, T. M.; Yang, S. *Langmuir* **2004**, *20*, 3824−3827.
(12) Voué, M.; Rioboo, R.; Adao, M. H.; Conti, J.; Bondar, A. I.; Ivanov, D. A.; Blake, T. D.; De Coninck, J. *Langmuir* **2007**, *23*, 4695−4699.
(13) Wang, K.-L.; Jones, T. B. *Langmuir* **2005**, *21*, 4211−4217.
(14) Blake, T. D.; De Coninck, J. *Langmuir* **2004**, *20*, 2977−2978.
(15) Miyama, M.; Yang, Y.; Yasuda, T.; Okuno, T.; Yasuda, H. K. *Langmuir* **1997**, *13*, 5494−5503.
(16) Fair, R. B. *Microfluid. Nanofluid.* **2007**, *3*, 245−281.
(17) Quinn, A.; Sedev, R.; Ralston, J. *J. Phys. Chem. B* **2003**, *107*, 1163−1169.
(18) Zhu, L.; Xu, J.; Xiu, Y.; Sun, Y.; Hess, D. W.; Wong, C.-P. *J. Phys. Chem. B* **2006**, *110*, 15945−15950.
(19) Verheijen, H. J. J.; Prins, M. W. J. *Langmuir* **1999**, *15*, 6616−6620.
(20) Kang, K. H. *Langmuir* **2002**, *18*, 10318−10322.
(21) Shapiro, B.; Moon, H.; Garrell, R. L.; Kim, C. J. *J. Appl. Phys.* **2003**, *93*, 5794−5811.
(22) Quinn, A.; Sedev, R.; Ralston, J. *J. Phys. Chem. B* **2005**, *109*, 6268−6275.
(23) Barberis, F.; Capurro, M. *J. Colloid Interface Sci.* **2008**, *326*, 201−210.
(24) Daub, C. D.; Bratko, D.; Leung, K.; Luzar, A. *J. Phys. Chem. C* **2007**, *111*, 505−509.
(25) Daub, C. D.; Bratko, D.; Luzar, A. *Top. Curr. Chem.* **2012**, *307*, 155−180.
(26) Bratko, D.; Daub, C. D.; Leung, K.; Luzar, A. *J. Am. Chem. Soc.* **2007**, *129*, 2504−2510.
(27) Bratko, D.; Daub, C. D.; Luzar, A.; Salmeron, M. *Faraday Discuss.* **2009**, *141*, 55−66.
(28) Nosonovsky, M.; Bhushan, B. *Nano Lett.* **2007**, *7*, 2633−2637.
(29) Dhindsa, M. S.; Smith, N. R.; Heikenfeld, J.; Rack, P. D.; Fowlkes, J. D.; Doktycz, M. J.; Melechko, A. V.; Simpson, M. L. *Langmuir* **2006**, *22*, 9030−9034.
(30) Han, Z.; Tay, B.; Tan, C.; Shakerzadeh, M.; Ostrikov, K. K. *ACS Nano* **2009**, *3*, 3031−3036.
(31) Wang, Z.; Ou, Y.; Lu, T.-M.; Koratkar, N. *J. Phys. Chem. B* **2007**, *111*, 4296−4299.
(32) Bonaccurso, E.; Kappl, M.; Butt, H.-J. *Curr. Opin. Colloid Interface Sci.* **2008**, *13*, 107−119.
(33) Butt, H.-J.; Cappella, B.; Kappl, M. *Surf. Sci. Rep.* **2005**, *59*, 1−159.
(34) Maali, A.; Bhushan, B. *J. Phys.: Condens. Matter* **2008**, *20*, 315201−315211.
(35) Guan, L.; Qi, G.; Liu, S.; Zhang, H.; Zhang, Z.; Yang, Y.; Wang, C. *J. Phys. Chem. C* **2009**, *113*, 661−665.
(36) Revilla, R.; Guan, L.; Zhu, X.-Y.; Yang, Y.-L.; Wang, C. *Langmiur* **2011**, *27*, 7603−7608.
(37) Xie, X. N.; Chung, H. J.; Sow, C. H.; Wee, A. T. S. *Mater. Sci. Eng., R* **2006**, *54*, 1−48.
(38) Jung, Y. C.; Bhushan, B. *Nanotechnology* **2006**, *17*, 4970−4980.
(39) Wenzel, R. N. *Ind. Eng. Chem.* **1936**, *28*, 988−994.
(40) Cassie, A. B. D. *Discuss. Trans. Faraday Soc.* **1948**, *3*, 11−16.
(41) Cassie, A. B. D.; Baxter, S. *Trans. Faraday Soc.* **1944**, *40*, 546−551.
(42) Maghsoudy-Louyeh, S.; Tittmann, B. R. *Colloids Surf., A* **2008**, *331*, 268−274.
(43) Butt, H.-J.; Kappl, M. *Adv. Colloid Interface Sci.* **2009**, *146*, 48−60.
(44) Papathanasiou, A. G.; Papathanasiou, A. T.; Boudouvis, A. G. *J. Appl. Phys.* **2008**, *103*, 034901.